Int J Adv Manuf Technol (2015) 81:2067–2086
DOI 10.1007/s00170-015-7310-0

ORIGINAL ARTICLE

Three-dimensional dynamic cutting forces prediction model during micro-milling nickel-based superalloy

Xiaohong Lu [1] · **Zhenyuan Jia** [1] · **Xinxin Wang** [1] · **Guangjun Li** [1] · **Zongjin Ren** [1]

Received: 7 July 2014 / Accepted: 13 May 2015 / Published online: 3 June 2015

Abstract Nowadays, there are urgent demands of micro structure/parts which have high strength in high-temperature environment in the fields such as aerospace, energy, power, biomedical, etc. Nickel-based superalloy with high strength and high hardness under high temperature is the suitable material for manufacturing this kind of micro parts. Aimed at the problem of the complicated cutting force variation rule when micro-end milling nickel-based superalloy, the cutting forces model during micro-end milling of nickel-based superalloy processing is studied. Firstly, micro-end milling hole experiments are carried out to establish the radical run-out prediction model of cutting edge, which lays the foundation for establishing the cutting thickness calculation model during micro-end milling. Then, based on the minimum cutting thickness value, micro-end milling of nickel-based superalloy process is divided into two different cutting processes: shear-dominant regime cutting process and ploughing-dominant regime cutting process. Moreover, cutting forces prediction model during shear-dominant regime cutting process is developed based on the cutting forces in proportion to cutting layer area, which takes the effect of ploughing into account. Meanwhile, cutting forces prediction model during ploughing-dominant regime cutting process is developed based on the cutting force in proportion to interference volume between the flank surface of cutting tool and the workpiece. The experiment results verify that the cutting forces prediction results and experiment results are well matched.

Keywords Micro-end milling · Nickel-based superalloy · Radial run-out of cutting edge · Minimum cutting thickness · Cutting forces model

1 Introduction

Due to the high strength, low thermal conductivity, high viscosity, liability to work hardening, difficulties of machining, and accuracy ensuring caused by carbide, nitride, and their compounds in nickel-based superalloy, Thakur et al. [1] declared that nickel-based superalloy is a typical difficult-to-cut material. So far, the scholars around the world have made many researches on the cutting forces during milling nickel-based superalloy process.

Alauddin et al. [2] built the average milling forces prediction model in forward and backward milling Inconel718 process and proved that the cutting force increases as the feed rate and axial cutting thickness increase and decreases as cutting speed decreases. Taking the size effect and radial run-out of the cutter into consideration, prediction model of nickel-based superalloy cutting force is established by Estrems et al. [3]. Parameter calibration of cutting force model is studied by Kuo and Ling [4], and three-dimensional cutting forces prediction model is built. Three-dimensional finite element simulation prediction model of high-speed milling Inconel718 is established by Soo and Dewes [5], and preliminary estimate shows that deviation of the prediction model is caused by inaccurate description of friction characteristics. Henderson et al. [6] thought that the effect of tool's round edge on cutting force is due to the friction between tool and part. The effects of

✉ Xiaohong Lu
lxhdlut@dlut.edu.cn

1 Key Laboratory for Precision and Non-traditional Machining Technology of Ministry of Education, Dalian University of Technology, 116024 Dalian, People's Republic of China

tool wear, the circular radius of cutting edge, and cutting parameters on cutting forces are taken into consideration to build cutting force model of milling nickel-based superalloy process. A nickel-based superalloy lathe experiment was conducted by Zhao et al. [7]. The cutting parameters of the experiment were rotation speed 60 r/min, feed rate 0.18 mm/r, and depth of cut 0.25 mm. The experiment results showed that the amount of tool wear is little, and the roughness of machined parts is less than Ra0.8 μm. Chun et al. [8] obtained the cutting parameters from the average cutting forces of machining, and they applied the cutting parameters to predict the variation of cutting force. Subrahmanyam et al. [9] presented a cutting force model for ball nose milling on inclined planes for given cutting conditions assuming a fresh or sharp cutter.

The machinability of nickel-based superalloy is testified by the related research results. The success of machining nickel-based superalloy with small depth of cut and roughness less than Ra0.8 μm provides a reference to the nickel-based superalloy micro-end milling. However, the size effect and minimum cutting thickness phenomena in micro-end milling process will bring about new theories and techniques; the macroscopic modeling theory of nickel-based superalloy is no longer suitable for the mesoscale machining process. Theoretical and modeling researches on cutting forces of nickel-based superalloy should be conducted based on the micro-scale characteristics.

At present, domestic and overseas scholars have performed many investigations on micro-end milling models for different materials during micro-end milling process. Cutting force model of micro-milling (part materials are NAK-55 steel, graphite, and aluminum alloy) was built by Bao and Tansel [10, 11], which considered the effects of feed rate per tooth, tool radius, tool run-out, and tool wear. A series of slot milling experiments on single ferrite base, pearlite base, multiphase ferrite, and pearlitic ductile iron were carried out by utilizing carbide end milling cutter with two flutes, whose diameter is 0.5 mm, by Vogler et al. [12]. There was a 12-kHz fluctuation signal, besides 500 Hz main shaft frequency and 1000 Hz cutting frequency, in the cutting force frequency spectrum which was conducted as slot milling nodular cast iron with 50 % of pearlite at the main shaft speed of 30,000 r/min and feed rate of 2 μm. For 48 m/min cutting speed caused by 3000 r/min main shaft speed, 12 kHz equates to 65.4 μm wavelength, which was close to the 70 μm average grain size of ferrite. And there was no signal above 10 kHz when cutting single ferrite or pearlite base nodular cast iron. The comparison showed that the multiphase micro structure caused fluctuation of cutting forces. The milling process was divided into two different cutting phases: ploughing-dominant part plastic deformation phase and shear-dominant chip forming phase by Li [13]. According to different cutting stages, milling force model was established. Through the analyses of micro-milling force when machining aluminum alloy and titanium alloy, characters and changing rules were gotten by Zhang [14].

Researches on micro-end milling forces model of steel, graphite, aluminum alloy, glass, and other materials offer reference to research on cutting forces model during micro-end milling nickel-based superalloy process. Nickel-based superalloy is a multiphase material, whose micro structure can cause fluctuation of cutting forces and make it difficult to predict fluctuation law of cutting forces during micro-end milling of nickel-based superalloy. Thus, the research on cutting forces model during micro-end milling of nickel-based superalloy process becomes one of the key issues to be solved.

2 Research on cutting edge total radical run-out in micro-end milling process

Most of the existing instantaneous cutting thickness models in micro-cutting process are based on the trochoid trajectories of cutting edge, which take spindle run-out and elastic recovery of workpiece into account but neglect the influences of cutter installation errors, cutter-holder manufacturing errors, system rigidity, and so forth on. The effect of cutter installation errors, cutter-holder manufacturing errors, spindle run-out, system rigidity, and so forth on the instantaneous cutting thickness ultimately comes down to the impact on instantaneous cutting thickness made by the total radical run-out of cutting edge with respect to the workpiece. Now, Malekian et al. [15], Filiz et al. [16], and Ahmadian and Nourmohammadi [17] used receptance coupling method to obtain the dynamic response functions of cutting edge in micro-cutting process, but this method is very complicated and is heavy on computations.

A new method of measuring total radical run-out of cutting edge is proposed in this paper. First, the total radical run-out of cutting edge is obtained based on the experiment, and the prediction model of the total radical run-out of cutting edge is established based on the experimental data. Then considering the effect of trochoid trajectories of cutting edge, total radical run-out of cutting edge, and minimum cutting thickness, the calculation models of the nominal instantaneous cutting thickness and cumulative instantaneous cutting thickness during the actual cutting process are established, and the single-tooth cutting phenomenon in micro-cutting process is analyzed. The research can make theoretical preparation for further study on micro-end milling force model.

2.1 Experiment design

On the self-developed micro CNC milling machine, as shown in Fig. 1, the influence of spindle rotation speed and extended

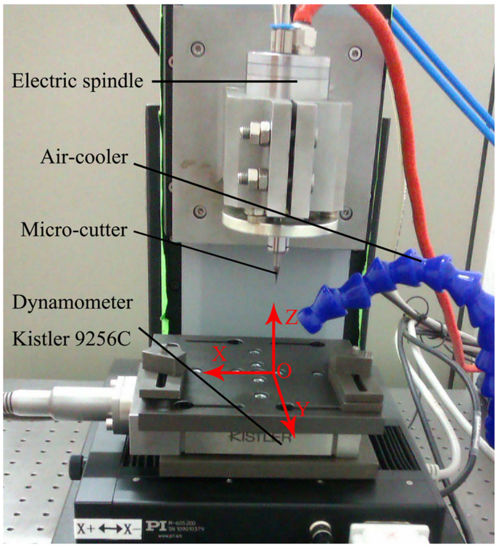

Fig. 1 The self-developed micro CNC milling machine

length of cutter (Fig. 2) on the cutting edge total radical run-out is studied by the experiment of micro-hole milling. Precise high-speed electric spindle is used in the self-developed micro-end milling machine, and the maximum rotational speed of the electric spindle is up to 140,000 rpm and the radical run-out of the spindle is less than 2 μm. The following experiments of micro-end milling slots are also conducted on this system.

Ultrafine particle-coated cemented carbide end milling tool with two flutes is used to mill micro-holes; the theoretical diameter of the milling tool is 0.6 mm, and the length of edge is about 0.5 mm; the tool nose radius is approximately 2.02 μm, and the helix angle is approximately 30°. The actual diameter measured by the scanning electron microscope is D= 594.1 μm (as shown in Fig. 3).

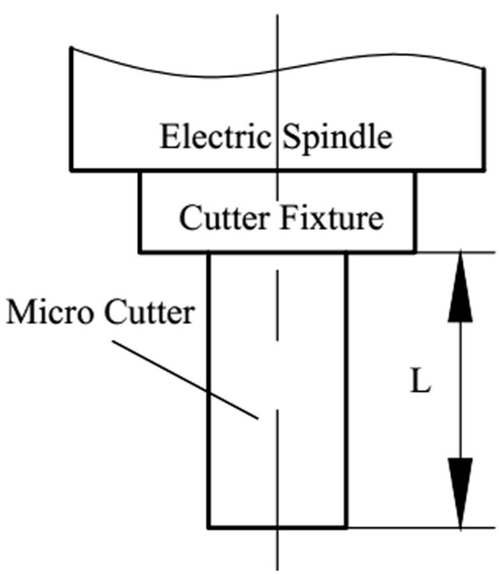

Fig. 2 Extended length of micro-end milling cutter

The material used is the typical difficult-to-machine material Inconel718, and the chemical composition and performance parameters are shown in Tables 1 and 2, respectively

The axial depth of micro-hole is 100 μm, and the axial feed rate is 0.01 mm/s. The cutter will be kept rotating in the micro-end milling hole for 30 s, when the point of cutter reaches the bottom of the hole during micro-end milling hole experimental process. It is assumed that the material's spring back effect can be removed when the cutter keeps rotating in the micro-end milling hole for 30 s. So the spring back effect can be neglected in the micro-milling experiments when modeling the magnitude of the total radial run-out. It is assumed that the effects of axial depth of cut, radial depth of cut, feed rate, and other factors to total radial run-out are neglected for the same cutting conditions, the same cutting tool, and the same machine tool.

The actual diameter of micro-end milling cutter is D, and the measured diameter of micro-hole is D_m, so the radical run-out of cutting edge is $r_0=(D_m-D)/2$.

Taking cutter extended length L and spindle speed n as experimental parameters, respectively, as shown in Table 3, the influence law of cutting edge total radical run-out by the various factors is analyzed. Thirty-six group experiments have been done, and in each group, five micro-holes are milled. Choose mean value of experiment results as the cutting edge total radical run-out under this rotational speed.

2.2 The experiment results and analysis

The experiment results of cutting edge total radical run-out under conditions of different experimental parameters are shown in Table 3.

Based on the experiment data in Table 3, a two-dimensional drawing plotted by MATLAB software is set forth, as shown in Fig. 4, which is about the cutting edge total radical run-out changes with cutter extended length and spindle speed.

2.3 Establish the prediction model of cutting edge total radical run-out

The prediction model of cutting edge total radical run-out is able to calculate arbitrary cutter extended length and spindle speed within the range of the experimental parameters. Use exponential Eq. (1) to fit experiment data and establish prediction model of cutting edge total radical run-out. In order to unite units, cutting edge total radical run-out with the unit millimeter is used to carry on the data fitting.

$$R_t = a \times L^b \times n^c \quad (1)$$

Where R_t is the total radical run-out of cutting edge (mm), a is the correction coefficient, and b,c is the impact index of cutter

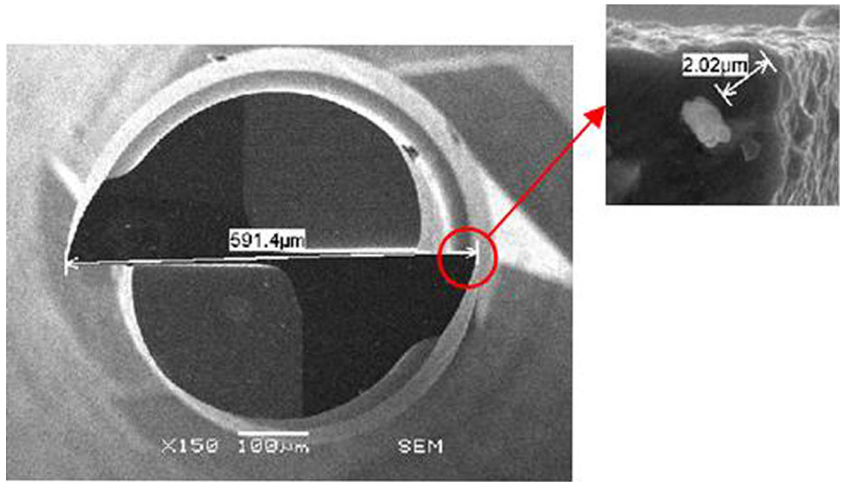

Fig. 3 The SEM photo of micro-end milling cutter

extended length and spindle speed to cutting edge total radical run-out.

Equation (1) is a nonlinear equation. To determine the coefficient, logarithmic transformation is used to turn it into a linear equation, as shown in Eq. (2). Based on the experiment data in Table 3, linear regress least square method is used to determine the coefficient of Eq. (2). The final solved prediction model is shown in Eq. (3).

$$\lg R_{\mathrm{t}} = \lg a + b \lg L + c \lg n \tag{2}$$

$$R_{\mathrm{t}} = 10^{-4.6477} \times L^{0.6080} \times n^{0.4182} \tag{3}$$

The F inspection is used to do significance test on regression equation and the variance analysis results are listed in Table 4.

The results of significant F inspection for regression equation is $F_{0.01}(2,33)=5.32<241.98$, so the prediction model of cutting edge total radical run-out is highly significant and relative fitting error of the regression equation is less than 0.0926. That the regression equation is highly significant merely suggests that it fits the experiment results well at the testing points, which cannot confirm that the calculated value fitting the measured value well within the whole range of the parameters. In order to confirm the effectiveness and accuracy of the established prediction model of cutting edge total radical run-out, 15 groups of experiment are designed to test the fitting degree of regression equation at 15 testing points within the region of parameters. Results of the comparison between measured value and theoretical calculated value of regression equation are represented in Table 5.

The F inspection is used to do fitting level test on regression equation, and the results are shown in Table 6: $F_{0.01}(25,8)=5.27>0.222$, so the regression equation of cutting edge total radical run-out fits well with the actual measured value.

So the established prediction model of cutting edge total radical run-out applies to the prediction of cutting edge total radical run-out in the range of $12 \le L \le 22$; $39680 \le n \le 92040$.

3 Analysis of characteristics of micro-milling process

Due to the sharp decline of machining characteristic scales during micro-end milling process, many assumptions made during traditional milling are invalid in micro-scale. Influences of cutter's round edge, the minimum cutting thickness, and elastic recovery of machined surface have been taken into consideration when analyzing the characteristics of micro-milling process.

3.1 The influence of cutter's round edge

Compared to traditional milling, rake face involved in milling reduces during micro-end milling process, so material removal is largely dependent on the area near cutting edge. In addition, due to the limit of micro tool machining technique, the size of the circular radius of cutting edge cannot decrease as processing scale reduces. The hypothesis that cutting edge is absolutely sharp is no longer valid during micro-milling by Wang [18]. Thus, the influence of cutter's round edge on micro-milling must be considered, as shown in Fig. 5.

Since cutting thickness is about the size of the arc radius of the cutting edge during micro-milling, the phenomenon of negative rake angle cutting can appear affected by the arc

Table 1 Chemical composition of Inconel718

Element	Ni	Fe	Cr	Mo	Ti	Nb	Al	Si	Co	Mn	Cu	C
Percent, %	48.42	19	19	3	0.9	5.3	0.5	0.35	3.0	0.35	0.1	0.08

Table 2 Performance parameters of Inconel718

Performance	Parameters
Density, kg/m^3	8470
Hardness, HRC	39~45
Modulus of elasticity, GPa	206
Poisson's ratio	0.3
Thermal conductivity, W/(m·K)	11.2
Yield stress, MPa	1110
Strain rate, %	23.3
Tensile strength, MPa	965

radius of the cutting edge. Due to the barrier of the negative rake, chips cannot flow smoothly along the rake face, friction characteristics between chips and rake face change, and ploughing effect between workpiece and flank surface increases. The lesser the cutting thickness, the more obvious the negative rake angle effect is and the more the influence on milling process. Meanwhile, the arc radius of the cutter is also one of the effects on the minimum cutting thickness.

3.2 The influence of the minimum cutting thickness

During micro-end milling process, the cutting thickness is usually at the same magnitude as the arc radius of the cutting edge, even smaller. Thus, the effect of cutting edge arc radius cannot be ignored when building micro-end milling forces prediction model during micro-end milling process. Flow of chips is impeded by arc radius of the cutting edge, which makes that not all tool teeth can form chips. Affected by tool geometrical parameters and material characteristics of workpiece, there is a critical thickness that can produce chips; Malekian et al. [19] named it the minimum cutting thickness. As it is shown in Fig. 6, when the actual cutting thickness is less than the minimum cutting thickness, there is elastic deformation between rear face of tools and workpiece surface, which results in no chip. When the actual cutting thickness is close to the minimum cutting thickness, both plastic deformation and elastic deformation occur, which result in cutting thickness accumulation phenomena. When the actual cutting thickness is more than the minimum cutting thickness and forces implemented on workpiece is close or above yielding limit of workpiece, plastic deformation will happen in cutting layer and is cut out as chips.

Table 3 The experiment results of cutting edge total radical run-out

L/mm R_t/μm n/(r/min)	12	14	16	18	20	22
39,680	8.97	9.55	9.55	10.58	12.3	13.0
49,600	9.43	10.23	10.73	11.08	13.51	13.12
59,520	9.88	11.6	11.53	12.42	14.35	14.7
69,440	10.35	12.42	13.57	13.0	15.4	15.4
79,370	11.02	13.68	13.68	13.84	16.1	16.1
92,040	11.6	14.7	14.35	15.05	16.33	17.8

Domestic and overseas scholars used experimental method, FEM method, and elastic-plastic theory analysis method to get the minimum cutting thickness during micro-end milling process. Their research results proved that the minimum cutting thickness was related to the arc radius of the cutting edge and friction characteristics between tool and workpiece. Microscopic mechanics strain gradient theory based on dislocation mechanism was proposed by Wu and Shi [20]. The minimum cutting thickness is supposed to be the cutting thickness corresponding to the internal stress of material that reaches critical stress of ductile fracture. The calculation equation of the minimum cutting thickness is

$$t_{\min} = r_e\left[1-\cos\left(\frac{180\times l}{2\pi\times r_e(\sigma_{\text{fracture}}/\sigma_{\text{JC}})^2}\right)\right] \tag{4}$$

Including

$$l = 18a^2G^2b/\sigma_{\text{JC}}^2 \tag{5}$$

$$\sigma_{\text{fracture}} = \frac{2(1-\nu)\times K_c{}^2}{\pi Gb} \tag{6}$$

l is the intrinsic characteristic length of material; a is a constant about 0.3 to 0.5; σ_{fracture} is the flow stress deduced by fracture mechanics when material is about to break; σ_{JC} is the material tensile reference stress; K_c is the stress intensity factor; ν is the Poisson ratio; G is the shear modulus; b is the modulus of Burgers vector; r_e is the arc radius of the cutting edge.

The minimum thickness Eq. (4) not only reflects the effect of the arc radius of the cutting edge on the minimum cutting thickness but also, based on micromechanics strain gradient theory, introduces material intrinsic characteristic length to represent the scale when material has the mesoscopic scale deformation. Equation (4) is used to calculate the minimum cutting thickness during micro-end milling.

Single-factor experiments are performed to prove the calculation of the minimum thickness. When cutting process transforms from plough-dominant regime cutting process to shear-dominant regime cutting process, there will be a peak of the maximum cutting force at the limit. The experiments are designed to prove the calculation of the minimum thickness. In the experiments, the spindle speed is 59,520 r/min, the axial depth of cut is 25 μm, the feed per tooth is changed, and the peak value of cutting force is measured. The feed per tooth is from 0.3 to 1.1 μm. The relationship between cutting force and feed per tooth is showed in Fig. 7.

Fig. 4 The influence rule of cutter extended length and spindle speed on the cutting edge total radical run-out

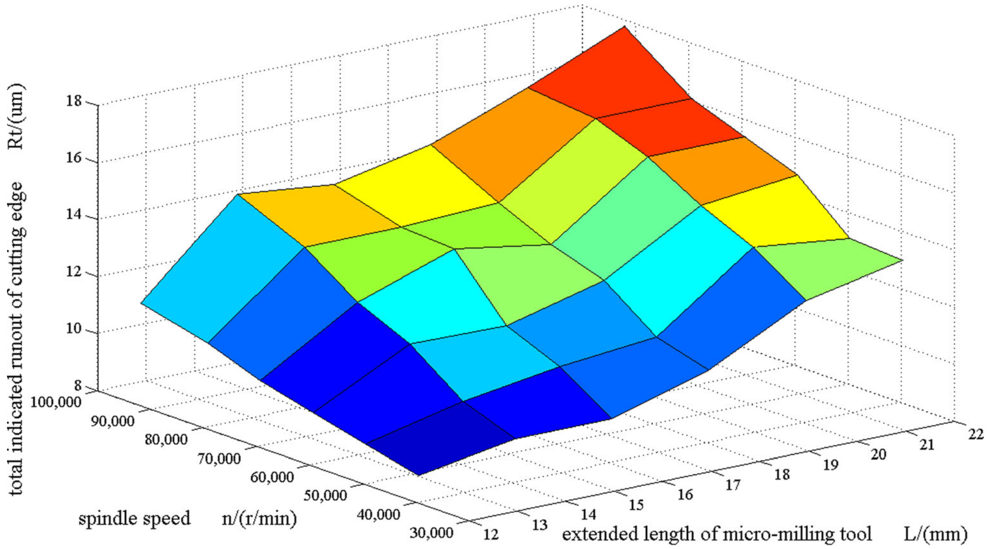

As shown in the figure, when the feed per tooth increases, the maximum cutting force increases at first then decreases. During the cutting process, the maximum cutting thickness is appropriately equal to feed per tooth. The minimum thickness should be equal to the feed per tooth where the peak appears. Therefore, the minimum thickness of the micro-milling Inconel718 process is 0.7 μm.

3.3 The influence of the elastic recovery of the machined surface

Affected by the arc radius of the cutting edge, during cutting process, there is a critical point where material separates. Material above this critical point forms chips by plastic deformation, while material below this critical point cannot be cut, and it is ironed by the cutting edge, detours the arc radius of the cutting edge, flows away along the rear face, and approaches to its original height by elastic deformation. This process is called ploughing effect. During the traditional cutting process, cutting forces are large; thus, the ploughing effect is not obvious, which is usually ignored. However, during micro-end milling process, the cutting thickness reduces sharply, which causes a significant effect on cutting forces. When the cutting thickness is small enough, the ploughing effect is dominant; thus, the influence of elastic recovery of the machined surface must be taken into account during micro-end milling process.

The calculation, formula (7), of the amount of elastic recovery put forward by Shi [21] is

$$\delta = \frac{3 \times \sigma_s}{4 \times E} \times r_e \times \left[2\exp\left(\frac{H}{\sigma_s} - \frac{1}{2}\right) - 1\right] \tag{7}$$

From formula (7), we can see that elastic recovery δ is decided by the radius of the cutting edge r_e, ratio between tensile strength of workpiece σ_s and elasticity modulus E, and ratio between hardness H and tensile strength of workpiece σ_s. There is an obvious linear relationship between elastic recovery and the radius of the cutting edge r_e.

Reduction of the cutting thickness makes the influence of the elastic recovery of the machined surface more obvious. The minimum cutting thickness t_{min} is regarded as the demarcation point of the elastic recovery in this paper. When the cutting thickness is larger than the minimum cutting thickness, the elastic recovery of the machined surface is supposed to be the largest, and then formula (8) can be used to calculate the amount of elastic recovery. When the cutting thickness is smaller than the minimum cutting thickness, the complete elastic recovery is supposed to happen on the machined

Table 4 The regression variance analysis table of total radical run-out regression equation

Sources of variance	Sum of squares	Degrees of freedom	Mean square deviation	F
Regression sum of squares	171.13	2	85.565	$\frac{85.565}{0.3536} \approx 241.98$
Residual sum of squares	11.67	33	0.3536	
Total deviations sum of squares	182.80	35	α=0.01	Highly significant

Table 5 Measured value and theoretical calculated value of the fitting degree testing points

R_t/um	13		17		21	
L/mm n	Measured	Calculated	Measured	Calculated	Measured	Calculated
39,680	9.14	8.97	10.26	10.56	12.55	12.00
59,520	10.72	10.63	12.43	12.51	14.42	14.22
79,370	12.15	11.98	13.81	14.11	16.09	16.04

surface. The amount of elastic recovery is approximately equal to the cutting thickness t_c. The calculation formula is shown below:

$$\left\{ \delta = \frac{3\times\sigma_s}{4\times E}\times r_e\times\left[2\exp\left(\frac{H}{\sigma_s}-\frac{1}{2}\right)-1\right] \quad t_c > t_{\min}\delta = t_c t_c \le t_{\min} \right. \tag{8}$$

4 Basic researches on cutting forces model during micro-end milling process

During micro-milling process, affected by the helix lead angle of the micro-end milling cutter's cutting edge, the instantaneous cutting forces on the cutting edge change continuously. Thus, the helix cutting edge cannot be simplified as an orthogonal turning tool to analyze. The part of cutting edge that is participating in cutting workpiece is divided into N infinitesimal with height of d_z. Each infinitesimal can be simplified as an orthogonal turning tool, regardless the effect of the helix lead angle. Infinitesimal cutting model during micro-end milling is built, and the forces of each infinitesimal bear are analyzed. The whole forces that the cutting edge bear can be gotten by accumulating the forces of all the infinitesimals bear. By accumulating the forces of all the cutting edge bear, the forces of the milling tool bear during cutting can be gained.

4.1 Geometrical model of micro-cutter edge

Ultrafine particle-coated cemented carbide end milling tool with two flutes is used, and the helix angle is about 30°. The studied micro-end milling forces prediction model is based on two coordinate systems, as shown in Fig. 8.

Rectangular coordinate system X-Y-Z is the static coordinate fixed on workpiece, while cylindrical coordinate system $\theta-r-h$ is the coordinate fixed on milling cutter and rotates with milling cutter. Z-axis coincides with h-axis. Origins of the two coordinates coincide. Cutter tooth position angle $\theta(t,k,z)$ is defined as the angle between projection of the line connecting the tooth tip of the k cutting edge with the cutter axis on x-y planes and the positive y-axis at time t. Clockwise is positive while counterclockwise is negative. The tooth position angle of the first cutting edge is assumed as zero, so the end tooth position angle of k cutting edge is

$$\theta(t,k) = 2\pi nt - \frac{2\pi k}{K} \tag{9}$$

t is time, k is the number of cutting edge, $k=0,1,2,\cdots,K-1$, and K is the total number of cutting edges.

Due to the effect of the helix angle, the tooth position angle of every point of the helical cutting edge is different from a lead or lag angle $\Phi_k(z)$ compared to the tooth position angle of the cutter's edge line. As shown in Fig. 8, this angle is the function of z-axis of this point:

$$\Phi_k(z) = \frac{z\times\tan\beta}{R} \tag{10}$$

During modeling, rotation direction of the cutter is clockwise. Taking the bottom of the first cutting edge line as reference, the position angle of infinitesimal of k cutting line with height of z at t moment is

$$\theta(t,k,z) = 2\pi nt + \frac{2\pi k}{K} - \frac{z\times\tan\beta}{R} \tag{11}$$

Due to the influence of the helix angle β, the actual cutting width of each infinitesimal dispersed

Table 6 The fitting degree test table of regression variance

Sources of variance	Sum of squares	Degrees of freedom	Mean square deviation	F
Lost fitness sum of squares	26.46	25	1.058	$\frac{1.058}{4.766}\approx 0.222$
Error sum of squares	38.13	8	4.766	
Total deviations sum of squares	221.46	44	$\alpha=0.01$	

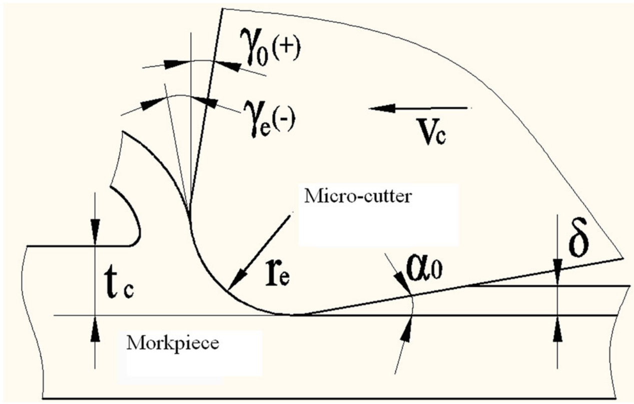

Fig. 5 Micro-cutting model with arc cutting edge

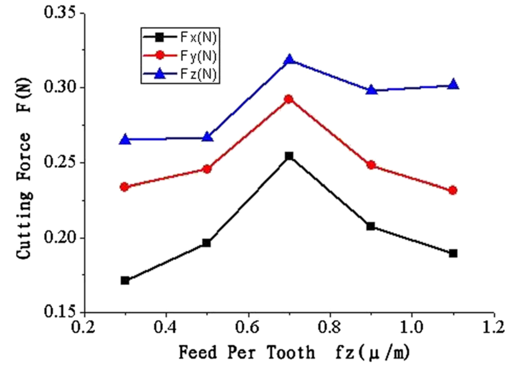

Fig. 7 Relationship between cutting force and feed per tooth

axially is not d_z but a bevel cutting width shown in Fig. 8.

$$d_{\mathrm{w}}=\frac{d_{z}}{\cos\beta}=\frac{R\times d\theta}{\sin\beta} \tag{12}$$

The track of cutting edge is dependent on tool radius, main shaft rotation speed, radial run-out of the cutting edge, and feed rate. The cutting edge trochoidal trajectory of the micro-end milling cutter is shown in Fig. 9. x is the direction of feed, and y is the perpendicular direction of feed direction. Cutter tooth position angle is defined as the angle between the line connecting the tooth tip with cutter axis and the positive y-axis. Clockwise is positive while counterclockwise is negative. Solid line is the cutting track of $k-1$ cutting edge, dashed line is the cutting track of k cutting edge, and dotted line is the track of cutter's axis. So the cutting track of k cutting edge changes with time t is:

$$\begin{cases} x(t,k)=ft+R\sin(\theta(t,k,z))+R_t\sin(\omega t+\varphi_0) \\ y(t,k)=R\cos(\theta(t,k,z))+R_t\cos(\omega t+\varphi_0) \\ z(t,k)=R\times\theta(t,k,z)/\tan\beta \end{cases} \tag{13}$$

Thereinto, f is the feed rate (mm/s); t is time (s); R is the radius of micro-milling cutter (mm); ω is the rotation speed of the main shaft (rad/s); k is the number of cutter, $k=0,1,2,\cdots,K-1$; K is the total number of cutters, in this paper, $K=2$; R_t is the radial run-out of the cutting edge (mm); and φ_0 is the initial angle of the radial run-out of the cutting edge (rad). The effect of the run-out of cutting edge is taken into account in this equation.

4.2 The determination of cut-in and cut-out angles of the cutter edge line

Since the existing of the helix angle of the cutter edge in the micro-end milling process, cut-in and cut-out angles of the cutting edge infinitesimals with different axial heights of a same edge line is different, namely, a lead or lag angle $\Phi_k(z)$ exists compared to the tooth position angle of the cutter's edge line. So, before building micro-end milling force prediction model, cut-in and cut-out angles at different time needs to be analyzed.

Two-edged, flat micro-end milling cutter is used in this paper to conduct slot milling experiment. Only one edge participates in cutting at any time. Cut-in and cut-out angles start at positive direction of y-axis (clockwise is positive while counterclockwise is negative). Figure 10a is the top view in axial direction. Figure 10b is the unfolded diagram along the cutter circumference direction; abscissa is the unfolded sketch of the milling cutter's outer circumference; ordinate is the axis direction of the milling cutter.

As it is shown in Fig. 10, during slot milling process, milling cutter rotates in clockwise. Lag angle Φ_{ap} of infinitesimal cutting edge at axial depth of cut a_p

Fig. 6 **a**, **b**, **c** Influence of the minimum cutting thickness

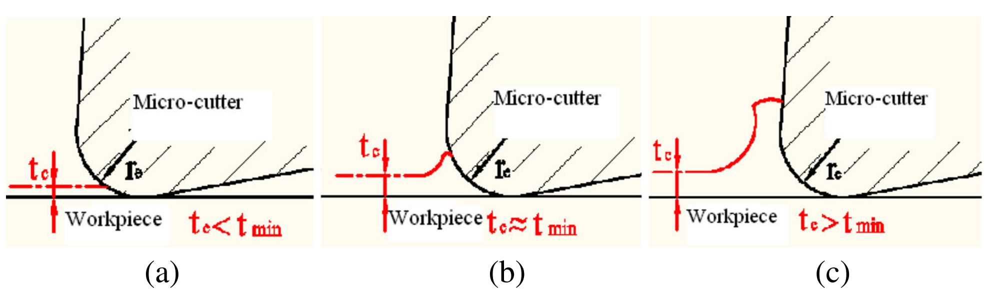

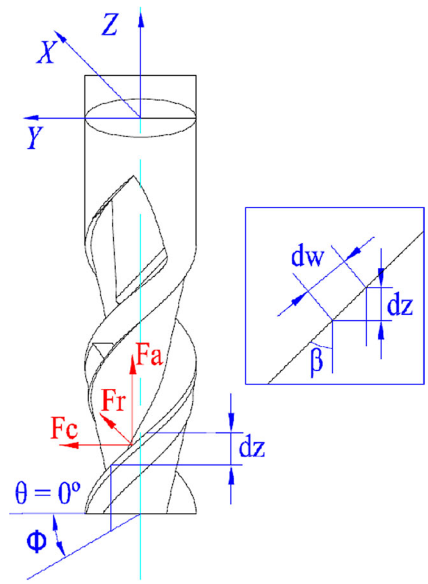

Fig. 8 The coordinate system for the micro-end milling forces prediction model

compared to infinitesimal cutting edge at the bottom of the cutter is

$$\Phi_{ap} = a_p \times \tan\beta / R \tag{14}$$

During slot-milling process, cut-in and cut-out angles are considered in the following three conditions, according to the tooth position angle $\theta_k(t,z)$:

1. When $0<\theta(t,k,z)<\Phi_{ap}$, as shown as line OA in Fig. 10b, cutting edge line cuts into workpiece from the end of the cutter as tooth position angle increases. The length of cutting edge line also increases gradually. So the cut-in angle $\theta_s=0$; cut-out angle $\theta_e=\theta_k(t,z)$.
2. When $\Phi_{ap}<\theta_k(t,z)<\pi$, as shown as line AB in Fig. 10b, cutting edge line below axial cutting depth all participates in cutting process within this range of the tooth position angle. So cut-in angle $\theta_s=\theta_k(t,z)-\Phi_{ap}$ and cut-out angle $\theta_e=\theta_k(t,z)$.
3. When $\pi<\theta_k(t,z)<\pi+\Phi_{ap}$, as shown as line BC in Fig. 10b, cutting edge line cuts out workpiece from the end of the milling cutter as the tooth position angle increases. So cut-in angle $\theta_s=\theta_k(t,z)-\Phi_{ap}$ and cut-out angle $\theta_e=\pi$.

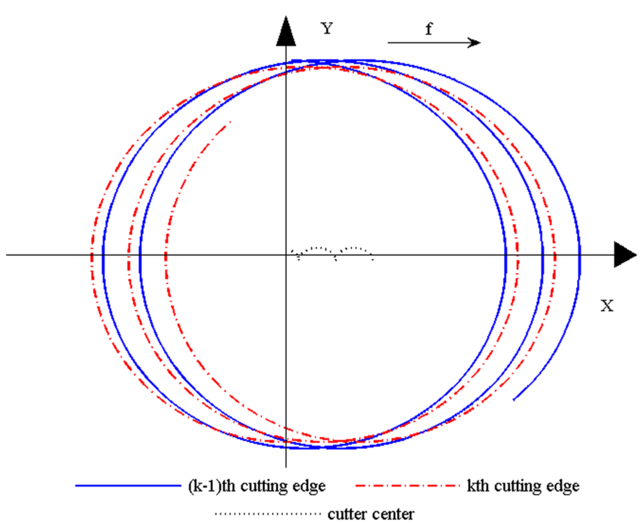

Fig. 9 The trochoid trajectory of cutting edge

4.3 The calculation of the area of cutting layer during micro-end milling

According to the traditional cutting theory, to two-edge milling cutter, two edges cut workpiece alternatively along the feed direction. The enveloped crescent area between the two cutting edge tracks represents the cutting thickness when cutting edge in touch with workpiece at this feeding process at various moments. As it is shown in Fig. 11, t_c is the instantaneous cutting thickness when the tooth position angle of k cutting edge is θ. Corresponding instantaneous cutting thickness is the single tooth feeding when the tooth position angle equals to 90°.

Judging from the sketch map of instantaneous cutting thickness, the nominal instantaneous cutting thickness t_c of the *kth* cutting edge at moment t is the length of line DE. Point D is the tracing point of no. $k-1$ cutting edge where tooth position angle is θ' at moment t'; point E is the corresponding cutting edge tracing point when no. k cutting edge passes point D at moment t; C' and C are, respectively, the centers of tool at moment t' and t. According to the geometric relationship of Fig. 11, instantaneous cutting thickness t_c of no. k cutting edge at moment t can be expressed as:

$$t_c = R + f_c \sin(\omega t - 2k\pi/K + \omega_0) - \sqrt{R^2 - f_c^2 \cos^2(\omega t - 2k\pi/K + \omega_0)} \tag{15}$$

Thereinto,

$$f_c = \sqrt{(x_c - x_{c'})^2 + (y_c - y_{c'})^2} \tag{16}$$

$$\omega_0 = \arctan((y_c - y_{c'})/(x_c - x_{c'})) \tag{17}$$

$$\begin{cases} x_{c'} = ft' + R_t \sin(\omega t' + \varphi_0) \\ y_{c'} = R_t \cos(\omega t' + \varphi_0) \end{cases} \tag{18}$$

$$\begin{cases} x_c = ft + R_t \sin(\omega t + \varphi_0) \\ y_c = R_t \cos(\omega t + \varphi_0) \end{cases} \tag{19}$$

Calculation model of instantaneous cutting thickness in Eq. (15) is nonlinear equation with two unknown time

Fig. 10 Sketch map to engagement angle of micro-cutter during micro-end milling. **a** To view in the tool's axial direction; **b** unfolded diagram along the circumference of the tool

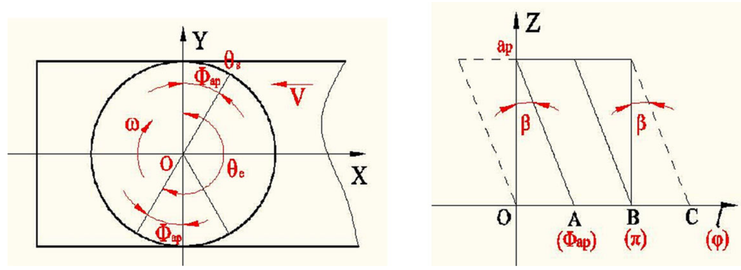

(a) To view in the tool's axial direction (b) Unfolded diagram along the circumference of the tool

quantities, so it needs to be solved by utilizing numerical solution method. Judging from Fig. 11, the key point of calculating instantaneous cutting thickness is to assure the collineation of points C, D, and E, namely, to deduce the moment t' when cutting edge reaches point D affects the calculation precision of cutting thickness model.

Micro-end milling process is a resultant motion of rotation of tool driven by main shaft and feed motion of workpiece. During slot-milling process, as cutting edge cuts in and cuts out workpiece, cutting thickness increases from zero to maximum and then from maximum to zero as the tool rotates. It is a nonlinear changing process. In axial direction, cutting thickness is constant with tooth position angle, while different cutting thicknesses differs corresponding to different tooth position angles. Cutting length involved in cutting process is different when cutting line cuts at different time and is also affected by the helix angle; even infinitesimal of the same cutting line corresponds to different cutting thicknesses. Thus, during micro-end milling process, the area of the cutting layer is different as the tool rotates. At moment t, the area $A(t,k)$ of cutting layer of number k cutting edge can be gotten by integral along cutting line.

$$A(t,k) = \int_{\theta_s}^{\theta_\varepsilon} \mathrm{t_c}(\mathrm{t},\mathrm{k},\theta) \times d\theta \tag{20}$$

Thereinto, $t_c(t,k,\theta)$ is the cutting thickness that different tooth position angles of number k cutting edge corresponds to at moment t. It can be solved by formula (16). The formula of $t_c(t,k,\theta)$ is so complicated that it is hard to get the results by integral function. Thus, it theoretically feasible to get area of cutting layer by formula (20), but not practical.

As it is shown in Fig. 10b, the cutting length of cutting edge is segmented when cutting in and cutting out workpiece, so subsection numerical integral method is used to get area of cutting layer.

During slot-milling process, the difference of arbitrary infinitesimal cutting edge cut-in angle and cut-out angle is π. The difference is divided into N parts, and the increment of each tooth position angle of infinitesimal is $\Delta\theta$:

$$\Delta\theta = \pi/N \tag{21}$$

Thus, when cutting edge cuts in and cuts out workpiece, tooth position angle of cutting edge infinitesimal is expressed as the following:

$$\theta_i = \theta_{i-1} + \Delta\theta \tag{22}$$

As shown in Fig. 10b, during the cutting process of OA and BC, the amount of infinitesimal division N_1 is

$$N_1 = \frac{\Phi_{\mathrm{ap}}}{\Delta\theta} = \frac{N \times a_{\mathrm{p}} \times \tan\beta}{\pi R} \tag{23}$$

As shown in Fig. 10b, instantaneous cutting layer thickness of OA, AB, and BC is expressed as the following when cutting edge involved in milling process when the tool cuts in and out workpiece:

$$\begin{cases} A(t_{\mathrm{j}}) = \dfrac{R \times \Delta\theta}{\sin\beta} \displaystyle\sum_{i=0}^{j} t_{\mathrm{c}}(\theta_i) & j \in [0, N^1] \quad (\mathrm{OA}) \\ A(t_{\mathrm{j}}) = \dfrac{R \times \Delta\theta}{\sin\beta} \displaystyle\sum_{i=j-N_1}^{j} t_{\mathrm{c}}(\theta_i) & j \in [N_1, {}^1N - N_1] \quad (\mathrm{AB}) \\ A(t_{\mathrm{j}}) = \dfrac{R \times \Delta\theta}{\sin\beta} \displaystyle\sum_{i=N-N_1}^{j} t_{\mathrm{c}}(\theta_i) & j \in [N - N_1, N] \quad (\mathrm{BC}) \end{cases} \tag{24}$$

Thereinto, $A(t_{\mathrm{j}})$ is the area of cutting layer corresponding to cutting edge involved in cutting process at moment t_{j}, and $t_{\mathrm{c}}(\theta_i)$ is the instantaneous cutting thickness when tooth position angle is θ_i; according to formula (15) of cutting thickness, $t_{\mathrm{c}}(\theta_i)$ can be expressed as:

$$t_{\mathrm{c}}(\theta_i) = t_{\mathrm{c}}(t_i) = R + f_{\mathrm{c}} \sin(\omega t_i + \omega_0) - \sqrt{R^2 - f_{\mathrm{c}}^2 \cos^2(\omega t_i + \omega_0)} \tag{25}$$

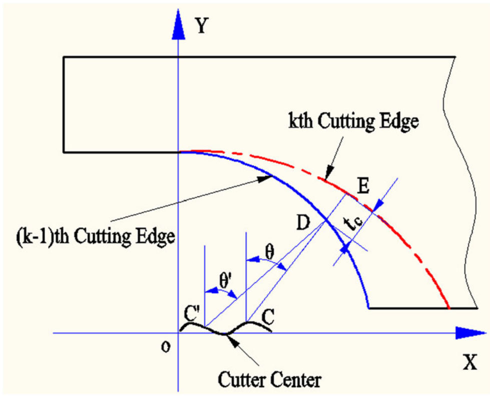

Fig. 11 The diagrammatic sketch of instantaneous cutting thickness

Thereinto, $t_i = t_{i-1} + \Delta t$; $t_1 = 0$ $i = 1,2,3\cdots\cdots N$

$$\Delta t = \frac{\Delta\theta}{2\pi n} = \frac{1}{2nN} \tag{26}$$

When numerical integral method is used to solve area of cutting layer corresponding to cutting edge involved in cutting process during micro-end milling process, the more precise the result is and the more tooth position angle divisions are. When N becomes infinity, the result can be approximately regarded as the area of cutting layer during actual cutting process.

5 Three-dimensional dynamic cutting forces prediction model

When actual cutting thickness is larger than the minimum cutting thickness during micro-end milling, cutting layer performs shear slipping plastic deformation under cutting force and is cut away as chips, namely, shear-dominant cutting process. When the actual cutting thickness is smaller than the minimum cutting thickness, the cutting layer, after being ironed by cutting edge, slips off flank surface of tool. Only elastic deformation occurs without any chip, which is called ploughing-dominant cutting process. When actual cutting thickness is close to the minimum cutting thickness, there will be accumulation of cutting thickness; thus, shear-dominant regime and ploughing-dominant regime both exist. Since there is a significant difference between shear-dominant regime and ploughing-dominant regime, and only one prediction model cannot describe these two cutting forces. The minimum cutting thickness is used as demarcation point during micro-end milling process in this paper. Cutting forces prediction model during shear-dominant cutting process and cutting forces prediction model during ploughing-dominant cutting process are built respectively.

5.1 Cutting forces prediction model during shear-dominant regime cutting process

When actual cutting thickness is larger than the minimum cutting thickness and cutting forces are over yield strength of the workpiece during micro-end milling, cutting layer performs shear slipping plastic deformation under cutting forces and is cut away in the form of chip removal. Deformation of cutting layer is mostly shear-dominant whose cutting mechanism is similar to traditional one. However, since cutting forces of micro-end milling is usually at millinewton magnitude, ploughing-dominant effect affects cutting process greatly. Thus, the effect of ploughing-dominant regime between flank face and machined workpiece surface on cutting forces cannot be ignored during shear-dominant regime cutting process. The influence of ploughing-dominant regime is not considered when building shear-dominant regime prediction model of cutting forces by Malekian et al. [15].

The influence of ploughing-dominant regime is considered during shear-dominant regime micro-end milling process. As elastic recovery of machined surface has been taken into account, cutting forces of ploughing-dominant regime is supposed to be in proportion to the interference volume between tool and the machined surface of workpiece. Axially discrete infinitesimal cutting forces prediction model of shear-dominant regime cutting process is built as the following:

$$\begin{cases} dF_r = \left(K_{rc} \times t_c(t,k,z) + K_{rp} \times A_p\right)\mathrm{dw} \\ dF_c = \left(K_{cc} \times t_c(t,k,z) + K_{cp} \times A_p\right)\mathrm{dw} \\ dF_a = \left(K_{ac} \times t_c(t,k,z) + K_{ap} \times A_p\right)\mathrm{dw} \end{cases} \quad (t_c > t_{min}) \tag{27}$$

dF_r, dF_c, and dF_a are the radial, tangential, and axial cutting forces of cutting edge infinitesimal with a unit of Newtons; K_{rc}, K_{cc}, and K_{ac} are the radial, tangential, and axial coefficient of shear-dominant regime cutting forces with a unit of Newton per square millimeter; K_{rp}, K_{cp}, and K_{ap} are the radial, tangential, and axial coefficient of shear-dominant regime cutting forces with a unit of Newton per cubic millimeter; A_p is the ploughing area with a unit of square millimeter; $t_c(t,k,z)$ is the instantaneous cutting thickness of infinitesimal of number k cutting edge on z-axis at moment t, which can be solved in formula (28) with a unit of millimeters; t_{min} is the minimum cutting thickness solved in formula (4) with a unit of millimeters; and dw is the cutting thickness of infinitesimal with a unit of millimeters.

Instantaneous accumulating cutting thickness of number k cutting edge at moment t is

$$\begin{cases} t_c(t,k) = t_c(t-2\pi/(\omega K), k-1) + t_c(t,k), & t_c(t-2\pi/(\omega K), k-1) < t_{min} \\ t_c(t,k) = t_c(t,k), & t_c(t-2\pi/(\omega K), k-1) \geq t_{min} \end{cases} \tag{28}$$

Since the radial, tangential, and axial forces of tool during micro-end milling cannot be measured directly, forces measured by dynamometer are forces of milling cutter on x-, y-, and z-axes. So cutting forces of infinitesimal, dF_r, dF_c, and dF_a, need to be decomposed to $X-Y-Z$ coordinate.

$$\begin{cases} dF_x = -dF_c \times \cos\theta - dF_r \times \sin\theta \\ dF_y = dF_c \times \sin\theta - dF_r \times \cos\theta \quad (t_c > t_{\min}) dF_z = dF_a \end{cases} \tag{29}$$

Thereinto, θ is tooth position angle of milling cutter, namely, the angle between line connecting tip of cutting edge and axis of milling cutter and positive direction of y-axis (clockwise is positive and counterclockwise is negative).

Three-dimensional cutting force of infinitesimal can be gotten by putting formulas (27) and (12) into formula (29):

$$\begin{cases} dF_x = -\dfrac{R}{\sin\beta}\left[\left(K_{cc} \times t_c(t,k,\theta) + K_{cp} \times A_p\right) \times \cos\theta + \left(K_{rc} \times t_c(t,k,\theta) + K_{rp} \times {A_p}^p\right) \times \sin\theta\right] d\theta \\ dF_y = \dfrac{R}{\sin\beta}\left[\left(K_{cc} \times t_c(t,k,\theta) + K_{cp} \times A_p\right) \times \sin\theta - \left(K_{rc} \times t_c(t,k,\theta) + K_{rp} \times {A_p}^p\right) \times \cos\theta\right] d\theta \\ dF_z = \dfrac{R}{\sin\beta}\left(K_{ac} \times t_c(t,k,\theta) + K_{ap} \times A_p\right) d\theta \end{cases} \tag{30}$$

Thereinto, $t_c > t_{\min}$

Cutting forces of a single miller cutter cutting edge can be obtained by integrating infinitesimal cutting forces along cutting edge. Cutting forces of milling cutter during shear-dominant regime micro-end milling process can be gained by accumulating cutting forces of K cutting edges. Its equation is

$$\begin{cases} F_x(t) = -\dfrac{R}{\sin\beta}\sum_{k=0}^{K-1}\int_{\theta_s}^{\theta_\varepsilon}\left[\left(K_{cc} \times t_c(t,k,\theta) + K_{cp} \times A_p\right) \times \cos\theta + \left(K_{rc} \times t_c(t,k,\theta) + K_{rp} \times {A_p}^p\right) \times \sin\theta\right] d\theta \\ F_y(t) = \dfrac{R}{\sin\beta}\sum_{k=0}^{K-1}\int_{\theta_s}^{\theta_\varepsilon}\left[\left(K_{cc} \times t_c(t,k,\theta) + K_{cp} \times A_p\right) \times \sin\theta - \left(K_{rc} \times t_c(t,k,\theta) + K_{rp} \times {A_p}^p\right) \times \cos\theta\right] d\theta \\ F_z(t) = \dfrac{R}{\sin\beta}\sum_{k=0}^{K-1}\int_{\theta_s}^{\theta_\varepsilon}\left(K_{ac} \times t_c(t,k,\theta) + K_{ap} \times A_p\right) d\theta \end{cases} \tag{31}$$

Thereinto, $t_c > t_{\min}$, and θ_e and θ_s are cut-in angle and cut-out angle of cutting edge, respectively.

Formula (31) is a three-dimensional dynamic model of cutting force when the actual cutting thickness is larger than the minimum cutting thickness. Six unknown quantities are calibrated by slot micro-end milling experiments.

When actual cutting thickness is larger than the minimum cutting thickness, shear-dominant regime is the main material deformation form. Meanwhile, considering the effect of ploughing-dominant regime between flank surface and workpiece, infinitesimal cutting model is as shown in Fig. 12.

In Fig. 12, δ is the elastic recovery of machined surface and its calculation formula is formula (8). Point S is the intersection of the minimum cutting thickness and arc of cutting edge, namely, material separation stagnation. Plastic slipping deformation of material happens in area above point S, while material ironed by cutting edge slips off flank surface in area below point S. Angle α_S between line

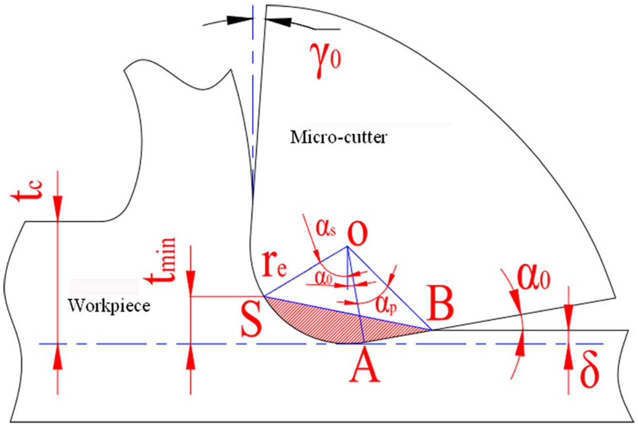

Fig. 12 Area of ploughing processing

connecting point S and arc center of cutting edge and y-axis is expressed as

$$\alpha_S = \cos^{-1}\left(\frac{r_e - t_{min}}{r_e}\right) \tag{32}$$

Thereinto, r_e is the arc radius of cutting edge whose unit is millimeters and t_{min} is the minimum cutting thickness with a unit of millimeters.

Shadow area A_p in Fig. 12 is the ploughing area between flank surface of tools and workpiece. According to geometrical relation, A_p is expressed as:

$$A_p = A_{AOS} + A_{AOB} - A_{BOS} \tag{33}$$

Thereinto, A_{AOS} is the area of sector AOS, A_{AOB} is the area of triangle AOB, and A_{BOS} is the area of triangle BOS.

The area of sector AOS is

$$A_{AOS} \approx \frac{1}{2} r_e^2 (\alpha_S + \alpha_0) \tag{34}$$

The area of triangle AOB is

$$A_{AOB} = \frac{1}{2} r_e \times l_{AB} \tag{35}$$

$$l_{AB} = \frac{\delta - r_e(1 - \cos\alpha_0)}{\sin\alpha_0} \tag{36}$$

The area of triangle BOS is

$$A_{BOS} = \frac{1}{2} r_e \times l_{BO} \times \sin(\alpha_S + \alpha_0 + \alpha_P) \tag{37}$$

$$l_{BO} = \sqrt{r_e^2 + l_{AB}{}^2} \tag{38}$$

$$\alpha_P = \tan^{-1}(l_{AB}/r_e) \tag{39}$$

When the cutting thickness is smaller than the minimum cutting thickness, the interference area A_p between flank surface and workpiece is expressed as

$$A_p = \frac{1}{2} r_e^2 (\alpha_S + \alpha_0) + \frac{1}{2} r_e \times l_{AB} - \frac{1}{2} r_e \times l_{BO} \times \sin(\alpha_S + \alpha_0 + \alpha_P) \tag{40}$$

5.2 Cutting forces prediction model during ploughing-dominant regime cutting process

When the actual cutting thickness is smaller than the minimum cutting thickness during micro-end milling process, cutting layer is firstly ironed by cutting edge then flows off the flank surface of tool. Only elastic deformation occurs without any chip, namely, ploughing-dominant cutting process. Using Malekian modeling theory, cutting force is supposed to be in proportion with interference volume of ploughing area during ploughing process. Ploughing-dominant regime model of cutting forces are developed as

$$\begin{cases} d\,F_r = (K_{rpp} \times A_p)\ \mathrm{d\,w} \\ dF_c = (K_{cpp} \times A_p)\ \mathrm{dw} \qquad t_c < t_{min}) \\ dF_a = (K_{app} \times A_p)\ \mathrm{dw} \end{cases} \tag{41}$$

K_{rpp}, K_{cpp}, and K_{app} are the radial, tangential, and axial coefficients of ploughing effect with a unit of Newton per cubic millimeter. Other parameters are the same as formula (27).

Formula (41) is decomposed into x, y, and z, three directions. Forces of three directions are expressed as

$$\begin{cases} dF_x = -\frac{R}{\sin\beta}\left[(K_{cpp} \times A_p) \times \cos\theta + (K_{rpp} \times A_p) \times \sin\theta\right]\ d\theta \\ dF_y = \frac{R}{\sin\beta}\left[(K_{cpp} \times A_p) \times \sin\theta - (K_{rpp} \times A_p) \times \cos\theta\right]\ d\theta \qquad t_c < t_{min}) \\ dF_z = \frac{R}{\sin\beta}(K_{app} \times A_p)\ d\theta \end{cases} \tag{42}$$

Cutting force of milling cutter during ploughing-dominant regime cutting process by integral of infinitesimal cutting forces along cutting edge is as follows:

$$
\begin{cases}
F_x(t) = -\dfrac{R}{\sin\beta}\displaystyle\sum_{k=0}^{K-1}\int_{\theta_s}^{\theta_\varepsilon}\left[\left(K_{\mathrm{cpp}}\times A_{\mathrm{p}}\right)\times\cos\theta+\left(K_{\mathrm{rpp}}\times A_{\mathrm{p}}\right)\times\sin\theta\right]\,d\theta \\
F_y(t) = \dfrac{R}{\sin\beta}\displaystyle\sum_{k=0}^{K-1}\int_{\theta_s}^{\theta_\varepsilon}\left[\left(K_{\mathrm{cpp}}\times A_{\mathrm{p}}\right)\times\sin\theta-\left(K_{\mathrm{rpp}}\times A_{\mathrm{p}}\right)\times\cos\theta\right]\,d\theta \qquad t_{\mathrm{c}}<t_{\min}) \\
F_z(t) = \dfrac{R}{\sin\beta}\displaystyle\sum_{k=0}^{K-1}\int_{\theta_s}^{\theta_\varepsilon}\left(K_{\mathrm{app}}\times A_{\mathrm{p}}\right)\,d\theta
\end{cases}
\tag{43}
$$

Formula (43) is a three-dimensional cutting forces prediction model when cutting thickness is smaller than the minimum cutting thickness. Three unknown quantities in the formula can be calibrated by slot-milling experiment.

As it is shown in Fig. 13, the shadow area is the ploughing area A_{p} when the actual cutting thickness is smaller than the minimum cutting thickness. The maximum elastic recovery δ is regarded as a node to get ploughing area in two situations.

As shown in Fig. 13a, when $\delta<t_{\mathrm{c}}<t_{\min}$, it is supposed that elastic recovery of machined surface is the maximum elastic recovery. Elastic recovery amount δ is calculated by formula (8). The calculation process of ploughing area is similar to that of shear-dominant regime ploughing area.

$$
A_{\mathrm{p}} = \frac{1}{2}r_{\mathrm{e}}^2(\alpha_{\mathrm{C}}+\alpha_0)+\frac{1}{2}r_{\mathrm{e}}\times l_{\mathrm{AB}}-\frac{1}{2}r_{\mathrm{e}}\times l_{\mathrm{BO}}\times\sin(\alpha_{\mathrm{C}}+\alpha_0+\alpha_{\mathrm{P}}) \tag{44}
$$

Thereinto,

$$
\begin{aligned}
\alpha_{\mathrm{C}} &= \cos^{-1}\left(\frac{r_{\mathrm{e}}-t_{\mathrm{c}}}{r_{\mathrm{e}}}\right)\\
l_{\mathrm{AB}} &= \frac{\delta-r_{\mathrm{e}}(1-\cos\alpha_0)}{\sin\alpha_0}\\
l_{\mathrm{BO}} &= \sqrt{{r_{\mathrm{e}}}^2+{l_{\mathrm{AB}}}^2}\\
\alpha_{\mathrm{P}} &= \tan^{-1}\left(\frac{l_{\mathrm{AB}}}{r_{\mathrm{e}}}\right)
\end{aligned}
\tag{45}
$$

As shown in Fig. 13b, when $t_{\mathrm{c}}<\delta<t_{\min}$, it is supposed that elastic recovery of machined surface is complete elastic recovery. Elastic recovery is close to cutting thickness. Ploughing area is expressed as:

$$
A_{\mathrm{p}} = \frac{1}{2}r_{\mathrm{e}}^2(\alpha_{\mathrm{D}}+\alpha_0)+\frac{1}{2}r_{\mathrm{e}}\times l_{\mathrm{AE}}-\frac{1}{2}r_{\mathrm{e}}\times l_{\mathrm{EO}} \times\sin(\alpha_{\mathrm{D}}+\alpha_0+\alpha_{\mathrm{Pe}}) \tag{46}
$$

Thereinto,

$$
\begin{aligned}
\alpha_{\mathrm{D}} &= \cos^{-1}\left(\frac{r_{\mathrm{e}}-t_{\mathrm{c}}}{r_{\mathrm{e}}}\right), \quad l_{\mathrm{AE}} = \frac{t_{\mathrm{c}}-r_{\mathrm{e}}(1-\cos\alpha_0)}{\sin\alpha_0}\\
l_{\mathrm{EO}} &= \sqrt{{r_{\mathrm{e}}}^2+{l_{\mathrm{AE}}}^2}, \quad \alpha_{\mathrm{Pe}} = \tan^{-1}\left(\frac{l_{\mathrm{AE}}}{r_{\mathrm{e}}}\right)
\end{aligned}
\tag{47}
$$

When the cutting thickness is smaller than the minimum cutting thickness, the interference volume A_{p} between flank surface of tool and workpiece are calculated as follows.

$$
\begin{cases}
A_{\mathrm{p}} = \dfrac{1}{2}r_{\mathrm{e}}^2(\alpha_C+\alpha_0)+\dfrac{1}{2}r_{\mathrm{e}}\times l_{\mathrm{AB}}-\dfrac{1}{2}r_{\mathrm{e}}\times l_{\mathrm{BO}}\times\sin(\alpha_{\mathrm{C}}+\alpha_0+\alpha_{\mathrm{P}})(\ \delta<t_{\mathrm{c}}<t_{\min}) \\
A_{\mathrm{p}} = \dfrac{1}{2}r_{\mathrm{e}}^2(\alpha_{\mathrm{D}}+\alpha_0)+\dfrac{1}{2}r_{\mathrm{e}}\times l_{\mathrm{AE}}-\dfrac{1}{2}r_{\mathrm{e}}\times l_{\mathrm{EO}}\times\sin(\alpha_{\mathrm{D}}+\alpha_0+\alpha_{\mathrm{Pe}})(t_{\mathrm{c}}<\delta<t_{\min})
\end{cases}
\tag{48}
$$

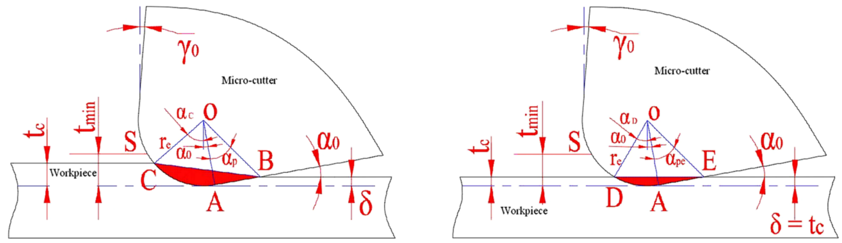

(a) $\delta < t_c < t_{min}$ (b) $t_c < \delta < t_{min}$

Fig. 13 Area of ploughing processing. **a** $\delta<t_c<t_{min}$; **b** $t_c<\delta<t_{min}$

5.3 Parameter identification of the cutting forces prediction model during micro-milling process

There are altogether nine coefficients of force in cutting force prediction model. Coefficient of shear effect indicates cutting force that cutting edge infinitesimal withstands when cutting chip per unit cutting layer area. Ploughing effect coefficient indicates cutting force that cutting edge infinitesimal withstands when there is unit interference volume between cutting edge infinitesimal and machined surface. Cutting force coefficients are related to geometrical parameters of tools, material of tool, and material of workpiece. For different tool materials and workpiece materials, cutting force coefficients are different, and thus, it is needed to conduct parameter identification before utilizing cutting force prediction model. Cutting force coefficients are approximately constant for the same tool material and workpiece material.

Cutting force coefficients of cutting forces prediction model formula (31) of shear-dominant regime and cutting force prediction model formula (43) of ploughing-dominant regime are constant, so cutting layer area and interference volume of ploughing area of certain tooth position angle involved in cutting edge can be gotten by subsection numerical integral. Cutting force of certain tooth position angle can be obtained by experiments. Based on data of cutting force and cutting layer areas, cutting force coefficients can be solved by least square method.

The following will take parameter identification of cutting force prediction model during shear-dominant regime as an example to analyze cutting force coefficient identification method. Cutting force coefficients at any time are supposed to be constant; then cutting force prediction model formula (31) during micro-end milling process is

$$\begin{cases} F_x(t) = -\left(K_{cc}\times A_c + K_{cp}\times V_c\right) - \left(K_{rc}\times A_s + K_{rp}\times V_s\right) \\ F_y(t) = \left(K_{cc}\times A_s + K_{cp}\times V_s\right) - \left(K_{rc}\times A_c + K_{rp}\times V_c\right) \\ F_z(t) = \left(K_{ac}\times A + K_{ap}\times V\right) \end{cases} \quad (t_c > t_{min}) \tag{49}$$

Thereinto,

$$\left\{ A_a = \frac{R}{\sin\beta}\sum_{k=0}^{K-1}\int_{\theta_s}^{\theta_\varepsilon} t_c(t,k,\theta)\ d\theta \qquad A_c = \frac{R}{\sin\beta}\sum_{k=0}^{K-1}\int_{\theta_s}^{\theta_\varepsilon} t_c(t,k,\theta)\ \cos\theta d\theta \qquad A_s = \frac{R}{\sin\beta}\sum_{k=0}^{K-1}\int_{\theta_s}^{\theta_\varepsilon} t_c(t,k,\theta)\ \sin\theta d\theta \right. \tag{50}$$

$$\left\{ V_a = \frac{R}{\sin\beta}\sum_{k=0}^{K-1}\int_{\theta_s}^{\theta_\varepsilon} A_p d\theta \qquad V_c = \frac{R}{\sin\beta}\sum_{k=0}^{K-1}\int_{\theta_s}^{\theta_\varepsilon} A_p\cos\theta d\theta \qquad V_s = \frac{R}{\sin\beta}\sum_{k=0}^{K-1}\int_{\theta_s}^{\theta_\varepsilon} A_p\sin\theta d\theta \right. \tag{51}$$

Based on cutting force prediction model formula (31) during micro-end milling process, cutting layer area of cutting edge line involved cutting at different tooth position angles is decomposed to x-y coordinate. Stimulation curve of half a period during tool rotation is shown in Fig. 14.

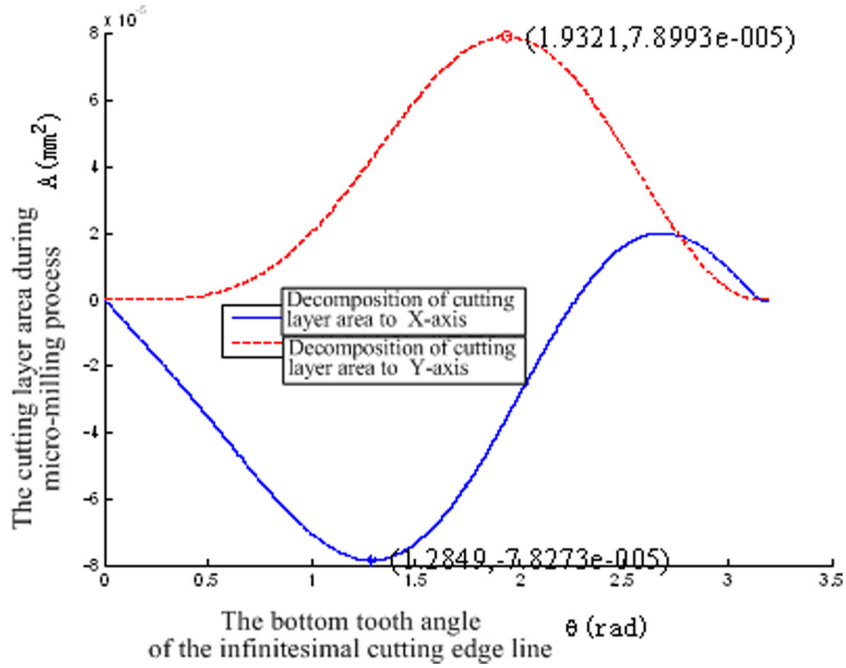

Fig. 14 Decomposition of cutting layer area to coordinate axes

Stimulation condition of Fig. 14 is the same as Fig. 12. Judging from Fig. 14, decomposition of cutting area to x-axis reaches a maximum when infinitesimal bottom tooth position angle of cutting edge line is 1.2849 radians, while the measured cutting force of x direction reaches its peak. Similarly, decomposition of cutting area to y-axis reaches a maximum when infinitesimal bottom tooth position angle of cutting edge line is 1.9321 radians, while the measured cutting force of y direction reaches its peak.

According to cutting forces prediction model of formula (50), cutting thickness is decomposed into A_c and A_s,as shown in Fig. 15.

Stimulation condition of Fig. 15 is the same as Fig. 14. Judging from Fig. 15, cutting force on x-axis reaches its peak when infinitesimal bottom tooth position angle of cutting edge line is 1.2849 radians. Summation of infinitesimal cutting layer area after decomposed is A_{cx}=2.0102×10^{-5} mm^2 and A_{sx}=6.1232×10^{-5} mm^2. Similarly, cutting force on y-axis

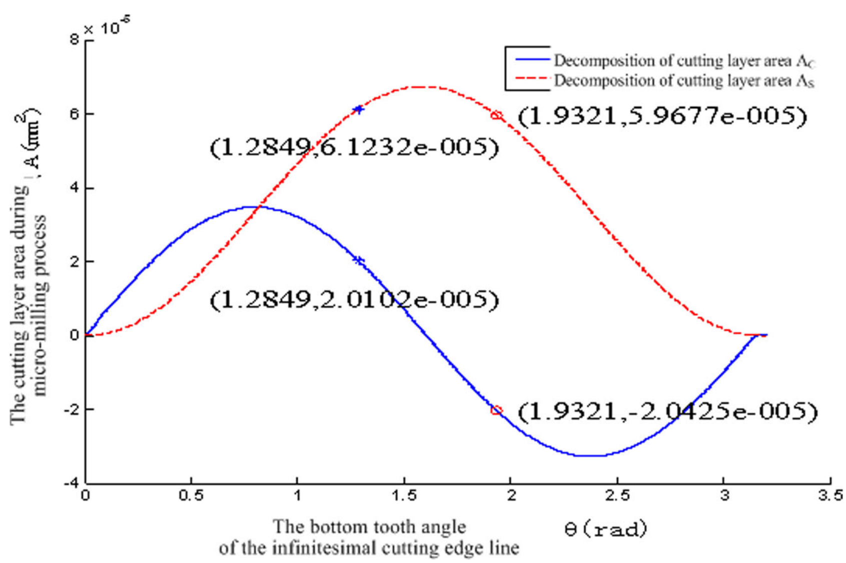

Fig. 15 Decomposition of cutting layer area

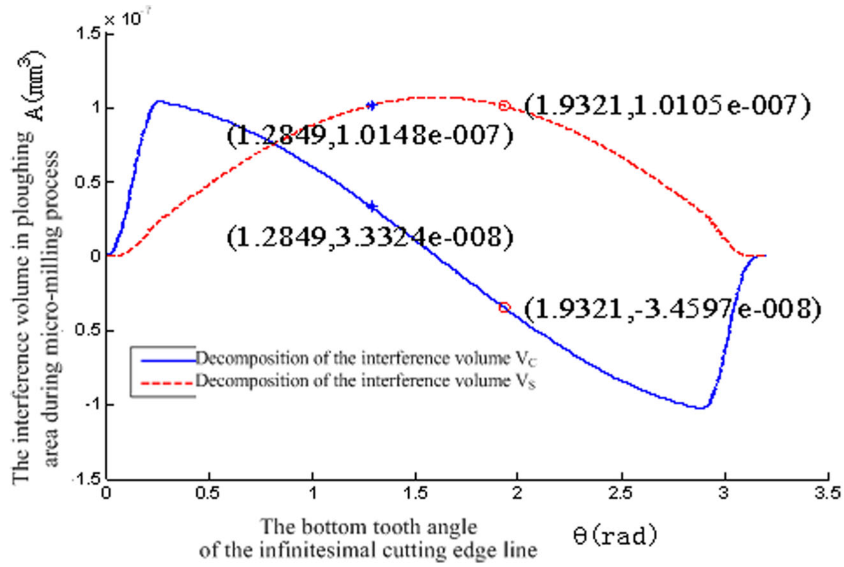

Fig. 16 Decomposition of interference volume in ploughing area

reaches its peak when infinitesimal bottom tooth position angle of cutting edge line is 1.9321 radians. Summation of infinitesimal cutting layer area after being decomposed is $A_{cy}=-2.0425\times10^{-5}$ mm², $A_{sy}=5.9677\times10^{-5}$ mm².

When the cutting thickness is smaller than the minimum cutting thickness, shear plastic deformation of material is dominant during cutting process, while ploughing effect between flank surface of cutting tool and workpiece cannot be ignored. Ploughing force is in proportion to interference volume of ploughing area. Based on cutting forces prediction model formula (51), interference volume of ploughing area is decomposed into V_c and V_s, as shown in Fig. 16.

Judging from Fig. 16, cutting force on x-axis reaches its peak when infinitesimal bottom tooth position angle of cutting edge line is 1.2849 radians. Summation of infinitesimal interference volume after being decomposed is $V_{cx}=3.3324\times10^{-8}$ mm³ and $V_{sx}=1.0148\times10^{-7}$ mm³. Similarly, cutting force on y-axis reaches its peak when infinitesimal bottom tooth position angle of cutting edge line is 1.9321 radians. Summation of infinitesimal interference volume after decomposed is $V_{cy}=-3.4597\times10^{-8}$ mm³ and $V_{sy}=1.9321\times10^{-7}$ mm³.

Supposing that when cutting layer area is maximum, axial force reaches its peak, $A_a=6.727\times10^{-5}$ N. The calculated ploughing volume is $V_a=9.23\times10^{-7}$ mm³.

Results of the experiment for identifying micro-cutting forces prediction model parameters in the shearing-dominant regime are shown in Table 7.

According to experimental condition of Table 7, parameter identification method proposed in this section is used to get cutting layer area and interference volume of ploughing area corresponding to cutting force prediction model, when x direction and y direction reach their peaks. The results are shown in Table 8.

Table 7 Results of the experiment for identifying micro-cutting forces prediction model parameters in the shearing-dominant regime

Serial number	Extended length L(mm)	Spindle speed n(r/min)	Axial depth of cut a_p(um)	Feed per tooth f_z(μm/z)	F_x(N)	F_y(N)	F_z(N)
1	12	69,440	30	0.9	0.2023	0.2546	0.3286
2	12	79,370	35	1.1	0.2579	0.29	0.4309
3	14	59,520	35	0.9	0.1873	0.2268	0.2991
4	14	69,440	15	1.1	0.1538	0.2137	0.3326
5	16	49,600	15	0.9	0.1215	0.1449	0.169
6	16	59,520	20	1.1	0.1556	0.1716	0.2042
7	18	39,680	20	0.9	0.1738	0.1897	0.24
8	18	49,600	25	1.1	0.217	0.2531	0.2516
9	20	39,680	30	1.1	0.1625	0.2281	0.2896
10	20	79,370	25	0.9	0.3511	0.4235	0.4538

Table 8 Cutting layer area and interference volume in ploughing area

Num.	$A_c(\times10^{-5}mm^2)$		$A_s(\times10^{-5}mm^2)$		$V_c(\times10^{-8}mm^3)$		$V_s(\times10^{-8}mm^3)$		$A_a(\times10^{-5}mm^2)$	$V_a(\times10^{-8}mm^3)$
	A_{cx}	A_{cy}	A_{sx}	A_{sy}	V_{cx}	V_{cy}	V_{sx}	V_{sy}		
1	1.6469	−1.6686	5.0164	4.8752	2.9421	−3.0545	8.959	8.9214	5.5045	10.687
2	2.3415	−2.3505	7.0953	6.9041	3.2613	−3.3453	9.8786	9.8474	7.79	11.88
3	1.9154	−1.9233	5.804	5.6491	3.3362	−3.4313	10.105	10.07	6.3735	12.152
4	1.0654	−1.0686	3.2275	3.1374	1.4344	−1.4753	4.3449	4.3312	3.5416	4.9256
5	0.8712	−0.8747	2.639	2.5683	1.5102	−1.5532	4.5743	4.5599	2.8975	5.1857
6	1.3911	−1.3831	4.1923	4.0822	1.8466	−1.8816	5.5642	5.5525	4.6041	6.4732
7	1.1273	−1.1419	3.4332	3.3357	1.9913	−2.0673	6.0636	6.0381	3.7666	7.0468
8	1.7045	−1.709	5.1642	5.0186	2.271	−2.3358	6.8791	6.8574	5.6663	8.1239
9	2.0318	−2.0379	6.124	5.9545	2.7792	−2.858	8.374	8.3474	6.7283	9.9991
10	1.4112	−1.3822	4.2306	4.1012	1.8383	−1.8556	5.5101	5.5043	4.6379	6.514

Based on data of Tables 7 and 8, cutting forces prediction model of formula (50) parameters in shear-dominant regime is solved by least squares estimation method. The results are $K_{cc}=5.8181\times10^3$, $K_{cp}=-1.1202\times10^6$, $K_{rc}=3.6715\times10^3$, $K_{rp}=-0.6803\times10^6$, $K_{ac}=7.3409\times10^3$, and $K_{ap}=-1.08258\times10^6$. Experiment results for identifying micro-cutting forces prediction model parameters in the ploughing-dominant regime are shown in Table 9.

By using model parameter identification method of this section, the calculated cutting forces model parameters in ploughing-dominant regime micro-end milling process are $K_{cpp}=3.3089\times10^6$, $K_{rpp}=0.4669\times10^6$, and $K_{app}=4.5218\times10^6$.

5.4 Experimental verification and analyses of the cutting forces prediction model

Cutting forces prediction model during micro-end milling of nickel-based superalloy process is testified by micro slot-milling experiment. Experiment conditions are two-edged flat end milling cutter, radius of milling cutter is 591.4 μm, rotating speed of shaft is 39,680 r/min, the extended length of tool is 20 mm, feed rate of each tooth is 1.1 μm, axial cutting thickness is 35 μm, and run-out calculated by prediction model of cutting edge run-out built in the previous section of the paper is 11.65 μm. Measured cutting forces curve and cutting forces curve predicted by cutting forces prediction model during slot-milling process are shown in Fig. 17.

As shown in Fig. 17a, instantaneous cutting force in X direction predicted by model matches well with experiment measured values. The change law of the predicted force and measured force is basically the same. As shown in Fig. 17b, the predicted cutting force peak values in Y direction match well with experiment measured peak values, while the main cutting force peak value of prediction model is a little smaller than experiment measured value. As shown in Fig. 17c, except that instantaneous predicted cutting forces peak values in Z direction match well with experiment measured peak values, other instantaneous cutting force values of prediction model are greater than experiment measured values. Judging from

Table 9 Experiment for identifying micro-cutting force prediction model parameters in the ploughing-dominant regime

Serial number	Extended length L(mm)	Spindle speed n(r/min)	Axial depth of cut a_p(um)	Feed per tooth f_z(μm/z)	F_x(N)	F_y(N)	F_z(N)
1	12	39,680	15	0.3	0.1214	0.1517	0.1515
2	12	49,600	20	0.5	0.1698	0.1884	0.1876
3	14	39,680	25	0.5	0.1551	0.1676	0.2198
4	14	79,370	20	0.3	0.1806	0.2799	0.3142
5	16	69,440	25	0.3	0.2104	0.2801	0.3274
6	16	79,370	30	0.5	0.2373	0.2635	0.3774
7	18	59,520	30	0.3	0.1867	0.2832	0.2577
8	18	69,440	35	0.5	0.279	0.4538	0.3237
9	20	49,600	35	0.3	0.1578	0.174	0.2744
10	20	59,520	15	0.5	0.1413	0.1548	0.2254

Fig. 17, valley values of *Y* and *Z* direction are greater than experiment measured values. The reasons of the discrepancies are comprehensive. The micro-milling force model ignores some of the factors that may influence cutting force, such as process damping and vibration of tool and workpiece. Process damping can reduce cutting force. Vibration is related to cutting thickness and it will sharpen the slope of the cutting force's curve. These factors of influence will be considered in the future studies. The other reason is the equipment error, such as the thermal drift of sensors and environment vibration. This kind of error cannot be controlled or eliminated completely.

The experiment results verify that dynamic prediction of variation period of instantaneous cutting forces during micro-end milling of nickel-based superalloy process and peak values can be realized by three-dimensional dynamic cutting force prediction model during micro-end milling of nickel-based superalloy that is developed in this paper.

Fig. 17 Experimental verification of three-dimensional dynamic cutting forces model. **a** Forces in *X* direction; **b** forces in *Y* direction

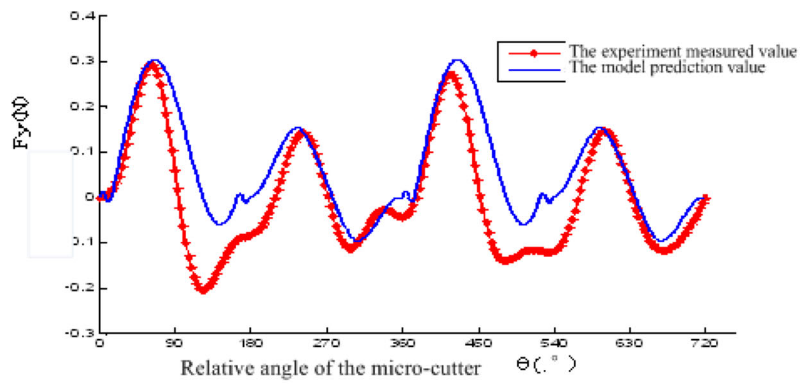

(a) Forces in X direction

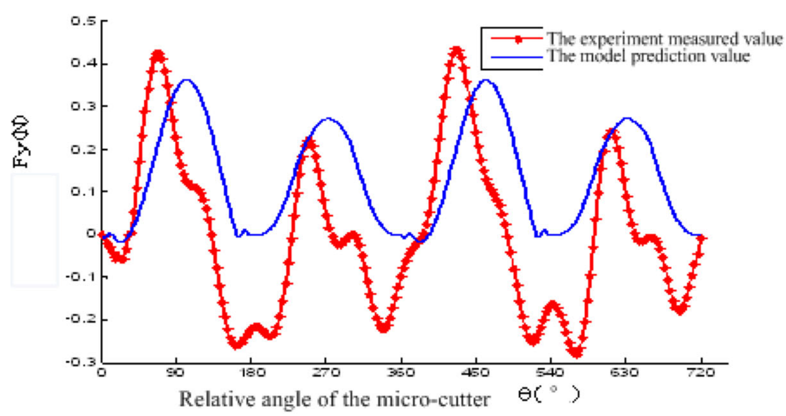

(b) Forces in Y direction

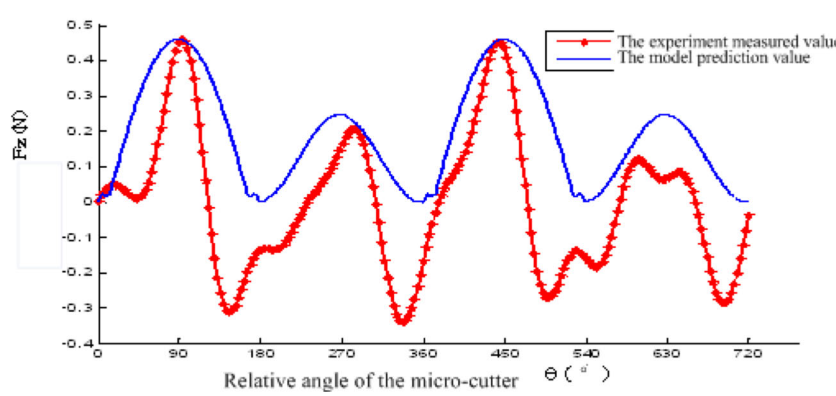

(c) Forces in Z direction

6 Conclusions

Based on the self-developed micro CNC milling machine, micro-milling groove orthogonal experiments are conducted to research on the cutting force during micro-milling the typical difficult-to-cut material Inconel718. Firstly, micro-milling hole experiments are carried out to research on the influence principle of extended length of cutter and spindle speed on the radial run-out of cutting edge. And the radical run-out prediction model of cutting edge is established according to experiment results, which lays the foundation for establishing the cutting thickness calculation model during micro-end milling. Secondly, the nominal cutting thickness calculation model during micro-end milling is established, with the consideration of the influence of trochoidal trajectory and radial run-out of cutting edge. In addition, the cumulative cutting thickness calculation model during actual cutting process is inferred, with the consideration of effects of single tooth cutting phenomenon and minimum cutting thickness phenomenon during micro-end milling process, which lays the foundation for establishing the three-dimensional dynamic cutting force prediction model. Thirdly, based on the minimum cutting thickness value, micro-end milling of nickel-based superalloy process is divided into two different cutting processes: shear-dominant regime cutting process and ploughing-dominant regime cutting process. Moreover, cutting force prediction model during shear-dominant regime cutting process is developed based on the cutting force in proportion to cutting layer area, which takes the effect of ploughing into account. Meanwhile, cutting force prediction model during ploughing-dominant regime cutting process is developed based on the cutting force in proportion to interference volume between the flank surface of cutting tool and the workpiece. The experiment results verify that the cutting forces prediction results and experiment results are well matched.

Acknowledgments This research is supported by the National Natural Science Foundation of China under Grant No. 51305061 and the Specialized Research Fund for the Doctoral Program of Higher Education under project number: 20120041120034. The financial contributions are gratefully acknowledged.

References

1. Thakur DG, Ramamoorthy B, Vijayaraghavan L (2009) Study on the machinability characteristics of superalloy Inconel 718 during high speed turning. Int J Mater Des 30(5):1718–1725
2. Alauddin M, Baradi MAE, Hashmi MSJ (1996) Modeling of cutting forces in end milling Inconel718. Int J Mater Process Technol 58:100–108
3. Estrems M, Sanchez HT (2011) Influence of size effect and radial run-outs on the end milling of a nickel-based superalloy. Trans N Am Manuf Res Inst SME 39:268–276
4. Kuo CP, Ling CC (2006) The prediction of cutting force in milling Inconel718. Int J Adv Manuf Technol 27(7–8):655–660
5. Soo SL, Dewes RC (2010) 3D FE modelling of high-speed ball nose end milling. Int J Adv Manuf Technol 50(9):871–882
6. Henderson AJ, Bunget C, Kurfess TR (2011) Cutting force modeling when milling nickel-base superalloys. J Proc ASME Int Manuf Sci Eng Conf 2010 2:193–202
7. Zhao XF, Wang YH, Liu Y, Wang XL, Wan Y (2010) Cutting of nickel-based high temperature alloy. J Aeronaut Manuf Technol 11: 46–50
8. Chun PK, Cheng CL, Shao HC, Chih WC (2005) The prediction of cutting force in milling Inconel-718. Int J Adv Manuf Technol 27: 655–660
9. Subrahmanyam KVR, Wong YS, Hong GS, Huang S (2010) Cutting force prediction for ball nose milling of inclined surface. Int J Adv Manuf Technol 48:23–32
10. Bao WY, Tansel IN (2000) Modeling micro-end-milling operations. Part II: tool run-out. Int J Mach Tools Manuf 40(15):2175–2192
11. Bao WY, Tansel IN (2000) Modeling micro-end-milling operations. Part III: influence of tool wear. Int J Mach Tools Manuf 40(15): 2193–2211
12. Vogler MP, Devfor RE, Kapoor SG (2003) Microstructure-level force prediction model for micro-milling of multi-phase materials. Int J Manuf Sci Eng Trans ASME 125(2):202–209
13. Li CF (2008) Study on fore and surface topography modeling and process optimization of meso-scale end-milling. Dissertation, Shanghai Jiaotong University
14. Zhang JF, Gong YD, Zhang YZ, Liu YM (2013) Experimental research and analysis on micro milling forces in process of high-speed micro-scale milling. J Northeast Univ (Natural Science) 34(2):284–287, **292**
15. Malekian M, Park SS, Jun MBG (2009) Modeling of dynamic micro-milling cutting forces. Int J Mach Tools Manuf 49(7):586–598
16. Filiz S, Cheng CH, Powell KB, Schmitz TL, Ozdoganlar OB (2009) An improved tool-holder model for RCSA tool-pint frequency response prediction. Int J Precis Eng 33:26–36
17. Ahmadian H, Nourmohammadi M (2010) Tool point dynamics prediction by a three-component model utilizing distributed joint interfaces. Int J Mach Tools Manuf 50(11):998–1005
18. Wang H (2009) Simulation study on mechanical characteristic and geometry of micro milling tool. Doctor Thesis. Dissertation, Nanjing University of Science and Technology
19. Malekian M, Mostofa MG, Park SS, Jun MBG (2012) Modeling of minimum uncut chip thickness in micro machining of aluminum. Int J Mater Process Technol 212(3):553–559
20. Wu JH, Shi ZY (2009) Minimum chip thickness in orthogonal micro-cutting based on plasticity strain gradient theory. J China Mech Eng 20(18):2227–2230
21. Shi WT (2011) Micro cutting technology. China Machine Press, Beijing